I N S T I T U T D ' A E R O N O M I E S P A T I A L E D E B E L G I Q U E

3 - Avenue Circulaire
B - 1180 BRUXELLES

AERONOMICA ACTA

A - N° 209 - 1979

A microscopic description of interpenetrated plasma regions

by

M. ROTH

B E L G I S C H I N S T I T U U T V O O R R U I M T E - A E R O N O M I E

3 - Ringlaan
B - 1180 BRUSSEL

FOREWORD

The paper entitled "A microscopic description of interpenetrated plasma regions" has been presented at the Sidney Chapman Conference on Magnetospheric Boundary Layers, 11-15 June 1979, held at Alpbach (Austria). It is published in the proceedings of this conference (ESA Scientific and Technical Publications, SP-148, 295-309, August 1979).

AVANT-PROPOS

Le travail intitulé "A microscopic description of interpenetrated plasma regions" a été présenté à la conférence Sidney Chapman sur les couches limites de la magnétosphère qui s'est tenue à Alpbach (Autriche) du 11 au 15 juin 1979. Il est publié dans les comptes-rendus de cette conférence (ESA Scientific and Technical Publications, SP-148, 295-309, August 1979).

VOORWOORD

De tekst getiteld "A microscopic description of interpenetrated plasma regions" werd voorgedragen tijdens de Sidney Chapman Conference on Magnetospheric Boundary Layers" welke plaats had te Alpbach (Oostenrijk) van 11 tot en met 15 juni 1979. Hij werd gepubliceerd in de verslagen van deze vergadering (ESA Scientific and Technical Publications, SP-148, 295-309, August 1979).

VORWORT

Diese Arbeit betitelt "A microscopic description of interpenetrated plasma regions" wurde zur Sidney Chapman Konferenz "Magnetospheric Boundary Layers" (11-15 Juni 1979) in Alpbach (Östereich) vorgetragen. Diese Arbeit ist in dem Vortrag dieser Konferenz veröffendlicht worden (ESA Scientific and Technical Publications, SP-148, 295-309, August 1979).

A MICROSCOPIC DESCRIPTION OF INTERPENETRATED PLASMA REGIONS

by

M. ROTH

Abstract

A model of steady-state tangential discontinuities has been developed using the kinetic theory of multi-components collisionless plasmas. In the momenta plane the velocity distribution functions are combined step functions of two anisotropic displaced Maxwellians whose first moments are identical with the actual asymptotic moments. We consider the magnetopause layer and the inner edge of the plasma boundary layer as regions where two different hydrogen plasmas are interpenetrated and the model is used to describe their microstructures. Large field-aligned currents are generated at the magnetopause and may constitute a part of the field-aligned currents observed in the cusps. A stability study shows that the electron layers are nearly always unstable. The thickness of stable ion layers increases with increasing values of the temperature ratio (T^+/T^-) and/or with decreasing density variations. This thickness represents also 2.5 ion gyroradii when (T^+/T^-) becomes larger than 5. A minimum magnetopause thickness is found equal to 100 km.

Key words : Vlasov plasmas, tangential discontinuities, modified two-stream instability, magnetopause, low latitude plasma boundary layer.

Résumé

Un modèle de discontinuités tangentielles stationnaires a été développé qui utilise la théorie cinétique des plasmas sans collisions à constituants multiples. Dans l'espace des impulsions, les fonctions de distribution des vitesses sont des fonctions étagées formées à l'aide de deux Maxwelliennes anisotropes et déplacées. Les premiers moments de ces Maxwelliennes sont identiques aux moments asymptotiques des actuelles fonctions de distribution. Nous considérons la magnétopause et le bord interne de la couche frontière plasmique comme des régions où deux plasmas d'hydrogène d'origine différente s'interpénètrent mutuellement et le modèle est utilisé pour en décrire leurs micro-structures. D'intenses courants alignés sont engendrés à la magnéto-pause et peuvent constituer une fraction des courants de Birkeland observés dans les cornets polaires. Une étude de stabilité montre que les couches électroniques sont presque toujours instables. L'épaisseur des couches ioniques augmente avec une augmentation du rapport de température (T^+/T^-) et/ou avec une diminution de la variation de densité. Cette épaisseur représente aussi 2,5 rayons de gyration ionique lorsque (T^+/T^-) devient plus grand que 5. On déduit une épaisseur minimale de la magnétopause égale à 100 km.

Mots-clés : Plasmas de Vlasov, discontinuités tangentielles, instabilité modifiée à deux faisceaux, magnétopause, couche frontière plasmique de basse latitude.

Samenvatting

Een stationair model voor tangentiële discontinuïteiten werd ontwikkeld steunend op de kinetische theorie voor botsingvrije plasmas opgebouwd uit meerdere bestanddelen. In de momenten-ruimte zijn de snelheidsverdelingsfuncties gegeven door een combinatie van twee anisotrope asymmetrische Maxwell-Boltzmann verdelingen waarvan de eerste orde momenten identiek zijn aan de asymptotische momenten van de eigenlijke snelheidsverdeling. De magnetopause en de inwendige rand van de plasma grenslaag worden beschouwd als zijnde een gebied waar twee verschillende soorten waterstofplasmas door elkaar dringen. De microstructuur hiervan wordt door het model beschreven. In de magnetopauze worden grote elektrische stromen langs de veldlijnen voortgebracht. Deze kunnen gedeeltelijk de Birkeland stromen waargenomen in de "Cusp" verklaren. Uit de studie blijkt ook nog dat de elektronenlagen bijna altijd onstabiel zijn. De dikte van de stabiele ionenlagen neemt toe met stijgende waarden van de temperatuursverhouding (T^+/T^-) en/of met afnemende dichtheidsvariaties. Indien (T^+/T^-) groter wordt dan 5 is deze dikte gelijk aan 2.5 gyrostralen. Het minimum in de dikte van de magnetopauze is ongeveer 100 km.

Zusammenfassung

Ein Modell für tangentielle Unterbrechungen ist entworfen worden. Die Kinetische Theorie für stossfreie Plasmas mehrerer Bestandteile ist gebraucht worden. Anisotrope Maxwellische Geschwindigkeitsverteillungen sind angenommen worden. Die ersten Momente dieser absturtzende Verteillungsfunktion sind den wirklichen Momenten gleich. Wir berechnen die Mikrostruktur der Magnetopause sowie der inneren Seite des "Plasma Boundary Layer" mit unserem Modell. Parallele elektrische Strömen enstehen in der Magnetopause und können eine substantielles Teil der Birkeland Strömen die in der "cleft" Ionosphäre beobachtet sind, betragen. Die elektronischen Schichten sind unstabil. Die Breite der Ionen Schichten wird grösser mit T^+/T^-. Diese Breite ist 2,5 mal die Ionen "Gyroradius" wenn $T^+/T^- > 5$. Die minimale Breite der Magnetopause ist 100 km.

1. INTRODUCTION

Cosmic plasmas are generally observed to divide themselves into distinct regions of different densities, temperatures, magnetizations and flow regimes. The boundaries of these regions are often stable transition layers with very high lifetimes, consisting of interpenetrated plasmas from the adjacent zones (Ref. 1). Most of these transitions contain electric sheet currents which change the orientation and the intensity of the magnetic field. Their observed thickness are generally of the order of a few ion Larmor gyroradii. In the Earth's environment, the neutral sheet, the magnetopause layer and the plasma boundary layer or even the filamentary structure of the solar wind are some of the most pertaining examples.

In this paper we shall use the kinetic theory of collisionless plasmas to describe the microstructure of a family of these boundary layers, i.e., tangential discontinuities. In Vlasov plasmas these types of layers have been studied by a number of authors. In this domain the work of Sestero (Ref. 2-3) is a pioneer one. This author considered tangential discontinuities in a magnetized hydrogen plasma with equal ion and electron temperatures. In this model the magnitude of the magnetic induction changes while the direction does not. Subsequently other models have been developed, some of them with the aim of describing the magnetopause structure : Alpers (Ref. 4) and Kan (Ref. 5) considered only exactly charge neutral sheet models, but included multidirectional currents in the plane of the discontinuity. Like Sestero the inclusion of a normal electric field has been investigated by Roth (Ref. 6) in a description of the plasmapause structure, by Lemaire and Burlaga (Ref. 7) in studies of tangential discontinuities in the solar wind, by Roth (Ref. 8) and more recently by Lee and Kan (Ref. 9) in descriptions of the magnetopause structure. All these latter models are generalizations of Sestero theory. They differ from one another in the

choice of the analytical forms used to represent the velocity distribution functions. This choice and the boundary conditions determine with uniqueness the microstructure of the boundary layers.

The model used in this paper is described in section 2. It allows the presence of a multi-components plasma and includes boundary conditions which permit plasma flows in the discontinuity plane and temperature anisotropies on both sides of the sheath. It differs only slightly from the previous model of Roth (Ref. 8) by inclusion of different mean velocities for the plasma constituents. In particular, two types of boundary layers can be derived compatibly with the presence of convection and charge separation electric fields. The first type includes layers in which the plasma bulk velocity on both sides is unchanged. In these layers the magnetic induction varies both in intensity and direction. The second type of layers includes structures in which the magnetic induction is everywhere oriented along a given direction. In these layers the magnetic induction varies only in intensity but the flow velocity changes both in intensity and direction.

In section 3 and 4 these two types of boundary layers are successively applied to the description of the microstructure of the magnetopause layer and inner edge of the plasma boundary layer. The role of ordinary and modified two-stream instabilities on the micro-stability and thickness of these current layers are analyzed in section 5 in the case of a hydrogen plasma. Main conclusions are given in section 6.

2. THEORY

2.1. Description of the model

In a collisionless plasma, a tangential discontinuity in the magnetic field is described by a kinetic theory based on the Vlasov-

Maxwell equations. In this model the plasma contains p components of different characteristics, each of them being identified with the superscript ν. The corresponding elementary particles have a mass $m^{(\nu)}$ and a charge $Z^{(\nu)}e$. (Here e is the proton charge). The plane of the discontinuity is parallel to the (y, z) plane and all the variables are assumed to depend on the x coordinate only. The plasma characteristics on opposite sides of the transition (at $x = -\infty$ and $x = +\infty$, identified with subscripts 1 and 2) are the main moments of the actual velocity distribution functions : number densities ($N_1^{(\nu)}$, $N_2^{(\nu)}$), mean velocity components ($V_{y_1}^{(\nu)}$, $V_{y_2}^{(\nu)}$ and $V_{z_1}^{(\nu)}$, $V_{z_2}^{(\nu)}$), perpendicular ($T_{\perp 1}^{(\nu)}$, $T_{\perp 2}^{(\nu)}$) and parallel ($T_{/\!/ 1}^{(\nu)}$, $T_{/\!/ 2}^{(\nu)}$) temperatures. Unlike components may be constituted of the same elementary particles. This can occur when two hydrogen plasmas (p = 4) of different energies and flow velocities are interpenetrated on both sides of the discontinuity.

Considering that there is no mass transfer across the transition and that the parallel conductivity is very large, the electric field is everywhere oriented along the x axis. Furthermore, the normal component of the magnetic field (B_x) is assumed to vanish since we do not consider rotational discontinuities. Therefore, the potentials of the electromagnetic field are inferred to be of the form (O, $a_y(x)$, $a_z(x)$) for the vector potential and $\phi(x)$ for the electrical potential.

2.2. Basic equations

In the rationalized MKSA units the Maxwell equations become

$$\frac{d^2 a_y}{dx^2} = - \mu_o \sum_{\nu=1}^{p} j_y^{(\nu)} \qquad (1)$$

$$\frac{d^2 a_z}{dx^2} = - \mu_o \sum_{\nu=1}^{p} j_z^{(\nu)} \qquad (2)$$

$$\frac{d^2\phi}{dx^2} = -\frac{e}{\varepsilon_o} \sum_{\nu=1}^{p} Z^{(\nu)}\, n^{(\nu)} \qquad (3)$$

where ε_o and μ_o are respectively the permittivity and the permeability of vacuum, $j_y^{(\nu)}$ and $j_z^{(\nu)}$ are the y and z components of the current density ($\vec{j}^{(\nu)}$) carried by the charged particles of the ν- species, and $n^{(\nu)}$ is the corresponding number density. The electric field (E, o, o) and the magnetic induction (O, B_y, B_z) derived from the electromagnetic potentials are given by

$$E = -\frac{d\phi}{dx} \qquad (4)$$

$$B_y = -\frac{da_z}{dx} \qquad (5)$$

$$B_z = \frac{da_y}{dx} \qquad (6)$$

The velocity distribution functions must satisfy Vlasov equation whose most general solution is any function depending only on the constants of particle motion. These constants are the kinetic energy (H) and the y and z components of the generalized momentum ($\vec{p}$)

$$H = \frac{1}{2m^{(\nu)}} (\vec{p} - Z^{(\nu)}\, e\, \vec{a})^2 + Z^{(\nu)}\, e\, \phi \qquad (7)$$

$$p_y = m^{(\nu)}\, v_y + Z^{(\nu)}\, e\, a_y \qquad (8)$$

$$p_z = m^{(\nu)}\, v_z + Z^{(\nu)}\, e\, a_z \qquad (9)$$

Here H is also the Hamiltonian of the particle while v_y and v_z are the y and z components of the particle velocity.

The structure of the transition is determined by solving the system of differential equations 1 to 6. This can be achieved by numerical methods when the current and number densities are expressed in terms of a_y, a_z and ϕ. The numerical integration is made possible by a method of predicator-corrector type (Ref. 10).

The electrical potential $\phi(x)$ satisfies Poisson equation 3. Its determination is greatly simplified by using the quasi-neutrality approximation

$$\sum_{\nu=1}^{p} Z^{(\nu)} \, n^{(\nu)} = 0 \qquad (10)$$

A self-consistent electric field is then obtained whenever the charge density $-\varepsilon_o \left(\frac{d^2\phi}{dx^2}\right)$ obtained by calculating the second derivative of the potential is much smaller than the charge density associated with the positive (or negative) charged particles. This condition being realized in most cases supports a priori the validity of approximation 10. To solve Eq. 10 we use Newton method of successive iterations.

2.3. The velocity distribution functions

From the previous paragraph it follows that the velocity distribution functions are any functions of H, p_y and p_z. In the present work we have generalized Sestero functions (Ref. 2-3) by using the following distributions :

$$F^{(\nu)}(H, p_y, p_z) = \sum_{i=1}^{2} \left\{ g_i^{(\nu)}(p_y, p_z) \cdot \eta_i^{(\nu)}(H, p_y, p_z) \right\} \qquad (11)$$

where $n_i^{(\nu)}$ are anisotropic displaced Maxwellians which will be later on stated while $g_i^{(\nu)}$ are discontinuous functions in the plane of the generalized momentum components. These latter functions take constant values $C_i^{(\nu)}$ (k) ($\geqq$ O) in each quadrant E_k(k = 1, 2, 3, 4) dividing this plane in four from a finite origin $\vec{p}_{o_i}^{(\nu)}$. For $Z^{(\nu)} > O$, these quadrants are defined in the following way :

$$E_1 =] - \infty, p_{oy_i}^{(\nu)}] \times [p_{oz_i}^{(\nu)}, + \infty [$$

$$E_2 = [p_{oy_i}^{(\nu)}, + \infty [\times [p_{oz_i}^{(\nu)}, +\infty [$$

$$E_3 =] - \infty, p_{oy_i}^{(\nu)}] \times] - \infty, p_{oz_i}^{(\nu)}]$$

$$E_4 = [p_{oy_i}^{(\nu)}, + \infty [\times] - \infty, p_{oz_i}^{(\nu)}]$$

For $Z^{(\nu)} < O$, quadrants E_1, E_4 and E_2, E_3 are permuted. This is illustrated in Figure 1 which shows that the asymptotic domains of quadrants E_k are related to the asymptotic values of the vector potential components located in the quadrants E_k' of the (a_y, a_z) plane. This can be easily seen from Eqs. 8-9 defining the generalized momentum components.

In what follows we shall always take

$$C_2^{(\nu)} (k_1) = 0 \qquad (12)$$

$$C_1^{(\nu)} (k_2) = 0 \qquad (13)$$

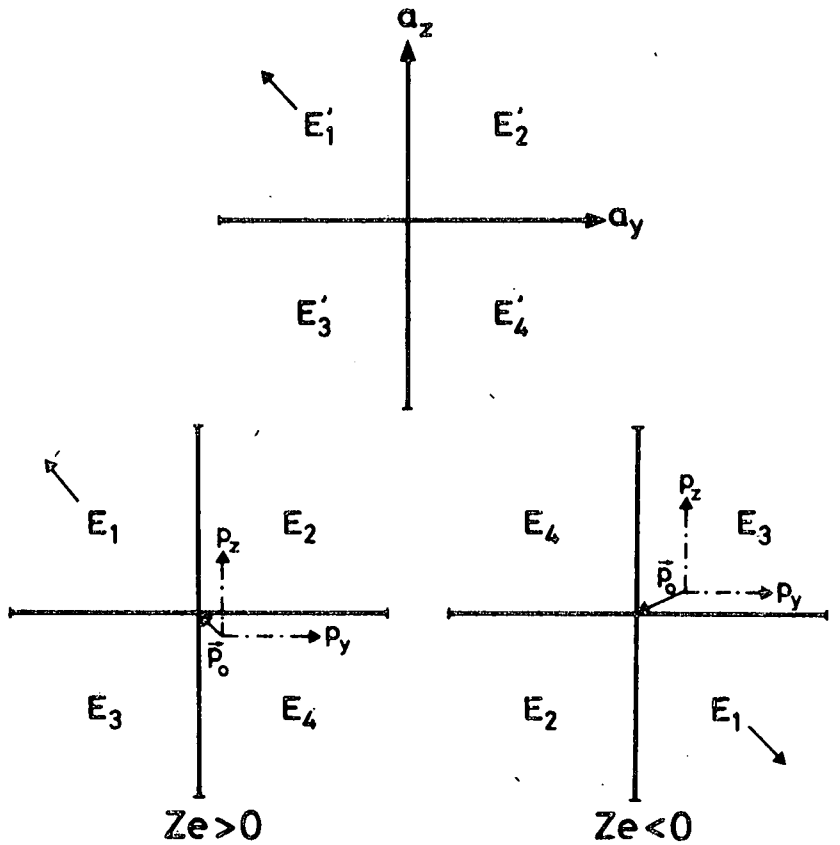

Fig. 1.- Definition of the quadrants E_k. For $\nu = 1, \ldots, p$ and $i = 1, 2$, these quadrants divide the generalized momenta plane (p_y, p_z) in four from a finite origin $\vec{p}_{oi}^{(\nu)}$. Quadrants E_1, E_4 and E_2, E_3 are permuted for charged particles of opposite signs as displayed by the figure. In this way, the asymptotic domains of quadrants E'_k dividing the (a_y, a_z) plane are related to the asymptotic domains of the corresponding quadrants E_k. This can be seen from the definition of the generalized momentum : $\vec{p} = m\vec{v} + Z\,e\,\vec{a}$. For example, the corresponding asymptotic domains of quadrants E'_1 and E_1 are indicated by arrows. When the vector potential curve starts in an asymptotic domain of a quadrant E'_{k_1} $(x = -\infty)$ and ends in an asymptotic domain of another quadrant E'_{k_2} $(x = +\infty)$, the velocity distribution functions change from their starting asymptotic forms in quadrants E_{k_1} to their final asymptotic forms in quadrants E_{k_2}, as defined by Eqs. 11 to 14.

$$C_1^{(\nu)}\ (k_1) = 1 \qquad (14)$$

Across the transition, from $x = -\infty$ ($i = 1$) to $x = +\infty$ ($i = 2$) the extremity of the vector potential describes a curve in the (a_y, a_z) plane starting in an asymptotic domain of a quadrant E'_{k_1} and ending in an asymptotic domain of another quadrant E'_{k_2}. Eqs. 11 to 14 then show that the velocity distribution function $F^{(\nu)}$ changes from $\eta_i^{(\nu)}$ at $x = -\infty$ to $C_2^{(\nu)}\ (k_2)\ \eta_2^{(\nu)}$ at $x = +\infty$. These asymptotic functions must have the same first order moments as the actual velocity distribution functions on each side. A simple description of these functions is given by anisotropic displaced Maxwellians of the form

$$\eta_i^{(\nu)}\ (H,\ p_y,\ p_z) = N^{(\nu)} \left(\frac{m^{(\nu)}}{2\pi k} \right)^{3/2} \frac{1}{T_{\perp i}^{(\nu)}\ T_{/\!/ i}^{(\nu)\ 1/2}} \cdot$$

$$\exp \left\{ - \frac{H}{kT_{\perp i}^{(\nu)}} \right\} \cdot \exp \left\{ - \frac{1}{kT_{\perp i}^{(\nu)}} \left[\frac{1}{2}\ m^{(\nu)}\ V_i^{(\nu)\,2} \right.\right.$$

$$\left.\left. - \vec{p} \cdot \vec{V}_i^{(\nu)} \right] \right\} \cdot \exp \left\{ - \frac{(A_i^{(\nu)} - 1)}{2m^{(\nu)}\ k\ T_{\perp i}^{(\nu)}} \cdot \right.$$

$$\left. \left[\sin \theta_i\ (p_y - m^{(\nu)}\ V_{y_i}^{(\nu)}) - \cos \theta_i\ (p_z - m^{(\nu)}\ V_{z_i}^{(\nu)}) + d_i^{(\nu)} \right]^2 \right\} \qquad (15)$$

where $A_i^{(\nu)}$ and $d_i^{(\nu)}$ are constants defined by

$$A_i^{(\nu)} = \frac{T_{\perp i}^{(\nu)}}{T_{\parallel i}^{(\nu)}} \qquad (16)$$

$$d_i^{(\nu)} = Z^{(\nu)} \, e \, a_{\parallel i} \qquad (17)$$

The constancy of $d_i^{(\nu)}$ is easily deduced from Eqs. 5-6. In Eq. 15, k is the Boltzmann constant and $N^{(\nu)}$ is a constant which will be shown related to the asymptotic number density at $x = -\infty$. The parameters θ_i are the constant angles between the z axis and the magnetic induction direction at $x = \mp \infty$. However, some conditions on the parameters entering into the definition of the asymptotic velocity distribution function given by Eq. 15 must be fulfilled to obtain charge neutrality and uniformity at $x = \mp \infty$. These conditions will be considered in the next section.

Finally, it could be shown that the velocity distribution functions defined in this paragraph have analytical moments of any order (Ref. 11). Their determination is purely algebrical but rather lengthy and will therefore not be considered here.

2.4. BOUNDARY CONDITIONS

2.4.1. Initial conditions

We start the integration with large initial values of the vector potential components situated in an asymptotic domain of quadrant E'_{k_1}. For these initial values the velocity distribution functions reduce to $\eta_1^{(\nu)}$. We also give initial values for the electrical potential and the magnetic induction components and assign an arbitrary negative value x_0 for the normal distance x. The constants $C_1^{(\nu)}(k_3)$, $C_1^{(\nu)}(k_4)$, $C_2^{(\nu)}(k_3)$ and $C_2^{(\nu)}(k_4)$ are suitably chosen to make the vector potential extremity describe a curve beginning and ending in prescribed quadrants E'_{k_1} and E'_{k_2}. This can be realized if the kinetic pressures

associated with the asymptotic domains of quadrants E_{k_3} and E_{k_4} are larger than the initial total pressure (kinetic + magnetic) associated with quadrant E_{k_1}. This procedure together with app. riate inital values of the vector potential components permits arbitrary rotations of the magnetic induction $\vec{B}$.

2.4.2. Constraints on the boundary conditions

At $x = \mp \infty$ the plasma and field parameters must become uniform. This implies some constraints on the parameters $\vec{V}_i^{(\nu)}$ and $N_i^{(\nu)}$. Indeed, the plasma must asymptotically be charge neutral and the total current density ($\vec{J}_i$) must vanish. This leads to the following conditions :

$$\sum_{\nu=1}^{p} Z^{(\nu)} N_i^{(\nu)} = 0 \qquad (18)$$

$$\sum_{\nu=1}^{p} Z^{(\nu)} N_i^{(\nu)} \vec{V}_i^{(\nu)} = 0 \qquad (19)$$

For different asymptotic mean velocities of plasma components the bulk velocity $\vec{c}_i$ is defined by

$$\vec{c}_i = \left(\sum_{\nu=1}^{p} N_i^{(\nu)} m^{(\nu)} \vec{V}_i^{(\nu)} \right) / \left(\sum_{\nu=1}^{p} m^{(\nu)} N_i^{(\nu)} \right) \qquad (20)$$

and the corresponding convection electric field is given by

$$\vec{E}_i = \vec{c}_i \wedge \vec{B}_i \qquad (21)$$

Eqs. 4 to 6 and Eq. 21 show that the asymptotic potentials take the following analytical forms :

$$\phi_i = \vec{a}_i \cdot \vec{c}_i + \phi_{o_i} \tag{22}$$

$$a_{y_i} = B_{z_i}\, x + a_{oy_i} \tag{23}$$

$$a_{z_i} = - B_{y_i}\, x + a_{oz_i} \tag{24}$$

where ϕ_{o_i}, a_{oy_i} and a_{oz_i} are constants which are generally different for $i = 1$ and $i = 2$.

We can determine the partial number densities and current densities at $x = - \infty$ ($i = 1$) and $x = + \infty$ ($i = 2$) by calculating the first moments of the asymptotic velocity distributions $C_i^{(\nu)}(k_i)\, \eta_i^{(\nu)}$. This gives the following results :

$$N_i^{(\nu)} = C_i^{(\nu)}(k_i)\, N^{(\nu)} \exp \left\{ - \frac{Z^{(\nu)} e\, (\phi_i - \vec{a}_i \cdot \vec{V}_i^{(\nu)}}{k\, T_{\perp i}^{(\nu)}} \right\} \tag{25}$$

$$\vec{J}_i^{(\nu)} = Z^{(\nu)}\, e\, N_i^{(\nu)}\, \vec{V}_i^{(\nu)} \tag{26}$$

Taking account of Eqs. 22 to 24, the dependence of Eq. 25 upon the electrical potential takes the following form :

$$\phi_i - \vec{a}_i \cdot \vec{V}_i^{(\nu)} =$$

$$[(\vec{c}_i - \vec{V}_i^{(\nu)}) \wedge \vec{B}_i]_x\, x + \vec{a}_{o_i} \cdot (\vec{c}_i - \vec{V}_i^{(\nu)}) + \phi_{o_i} \tag{27}$$

For the plasma to remain uniform, it is therefore essential that

$$\vec{V}_i^{(\nu)} = \vec{c}_i - \alpha_i^{(\nu)} \vec{B}_i/B_i \tag{28}$$

where $\alpha_i^{(\nu)}$ are constants which must satisfy Eqs. 19-20. When $\vec{V}_i^{(\nu)}$ are given by Eq. 28 the dependence of Eq. 25 upon the electrical potential reduces to :

$$Z^{(\nu)} e \, (\phi_i - \vec{a}_i \cdot \vec{V}_i^{(\nu)}) = \alpha_i^{(\nu)} d_i^{(\nu)} + Z^{(\nu)} e \, \phi_{o_i} \tag{29}$$

In this paper we shall analyze a class of transitions for which

$$\vec{V}_1^{(\nu)} = \vec{V}_2^{(\nu)} \tag{30}$$

$$\alpha_i^{(\nu)} \, d_i^{(\nu)} = 0 \tag{31}$$

Eq. 30 indicates that the mean velocity of any plasma component is unchanged on both sides of the transition while Eq. 31 shows that the asymptotic densities are given by

$$N_i^{(\nu)} = C_i^{(\nu)} \, (k_i) \, N^{(\nu)} \exp \left(- \frac{Z^{(\nu)} e \, \phi_{o_i}}{k \, T_{\perp i}^{(\nu)}} \right) \tag{32}$$

In a frame of reference moving with the velocity $\vec{c}_1$ we normalize the electrical potential to zero, i.e.,

$$\phi_{O_1} = 0 \tag{33}$$

Taking account of Eq. 14 the constants $N^{(\nu)}$ are then seen equal to the number densities at $x = -\infty$, i.e.,

$$N_1^{(\nu)} = N^{(\nu)} \tag{34}$$

In a frame of reference moving with the bulk velocity of the plasma the electrical potential difference ϕ_{O_2} is deduced from Eq. 32

$$\phi_{O_2} = - \frac{k_{\ell} T_2^{(1)}}{Z^{(1)} e} \ln \left[\frac{N_2^{(1)}}{C_2^{(1)}(k_2)\, N_1^{(1)}} \right] \tag{35}$$

The superscript (1) identifies an arbitrary first plasma constituent. From Eq. 35, it is seen that the value of the constant $C_2^{(1)}(k_2)$ determines the electrical potential difference ϕ_{O_2}. The other constants $C_2^{(\nu)}(k_2)$ are given by

$$C_2^{(\nu)}(k_2) = \frac{N_2^{(\nu)}}{N_1^{(\nu)}} \left[\frac{N_2^{(1)}}{C_2^{(1)}(k_2)\, N_1^{(1)}} \right]^{- \frac{Z^{(\nu)}\, T_{\ell 2}^{(1)}}{Z^{(1)}\, T_{\ell 2}^{(\nu)}}} \tag{36}$$

When the quantities $\sum_{i=1}^{2} C_i^{(\nu)}(k_j)$, $j = 1, \ldots, 4$ are equal to unity and $\eta_1^{(\nu)} = \eta_2^{(\nu)}$, the corresponding velocity distribution function remains a

full Maxwellian throughout the transition and the temperatures and mean velocity of this constituent remain constant from $x = -\infty$ to $x = +\infty$. When electron (resp. ion) constituents remain Maxwellian distributed the ions (resp. electrons) alone contribute to the variation of the magnetic induction. As Sestero [Ref. 2] we have called this type of transitions 'ion (resp. electron) layers'. Notwithstanding this distinction the class of transitions defined by Eqs. 30-31 can be split up into two categories which will be described in the next two sections.

2.5. Transitions for which $\vec{c}_1 = \vec{c}_2$, $\vec{B}_1 \neq \vec{B}_2$, $B_1 \neq B_2$)

If $\alpha_i^{(\nu)} = 0$, Eq. 31 is satisfied and Eq. 28 indicates that at $x = \mp \infty$ all the plasma components move with the same mean velocity equal to the bulk velocity. Furthermore, Eq. 30 states that the bulk velocity must remain unchanged at $x = -\infty$ and $x = +\infty$.

If $d_1^{(\nu)} \neq 0$ ($\alpha_1^{(\nu)} = 0$), the initial parallel component of the vector potential is not vanishing. A large series of computations has shown that the value of $a_{\parallel 0_1}$ is a parameter controlling the total rotation ($\Delta\theta$) of the magnetic induction. However, arbitrary rotation of $\vec{B}$ can be made possible principally by choosing suitable starting (E'_k) and ending (E'_k) quadrants and suitable values of the constants $C_i^{(\nu)}(k_3)$ and $C_i^{(\nu)}(k_4)$ as described in section 2.4.1. With this procedure $\Delta\theta$ can take arbitrary values in any quadrant between 0 and 2π. Subsequently, the value of $a_{\parallel 0_1}$ controls the rotation in this quadrant. For these transitions, parallel currents are generated since the magnetic induction changes direction. When the magnetic induction is rotating throughout the transition its final orientation is not known a priori and we restrict the model to isotropic temperatures at $x = +\infty$ (i.e., $A_2^{(\nu)} = 1$). This reduces to unity the last exponential term of $\eta_2^{(\ )}$ defined in Eq. 15 and avoid tedious iterations to determine the true value of $d_2^{(\nu)}$ (or $a_{\parallel 2}$).

2.6. Transitions for which $\vec{c}_1 \neq \vec{c}_2$ ($c_1 \neq c_2$), $\vec{B}_2 \propto \vec{B}_1$

These transitions allow a variation in intensity and direction of the plasma bulk velocity while the magnetic induction remains everywhere oriented along a given direction. This category of boundary layers are constructed by taking $d_i^{(\nu)} = 0$, i.e., $a_{\parallel 0_1} = a_{\parallel 0_2} = 0$. In this case Eq. 31 is satisfied even if $\alpha_i^{(\nu)} \neq 0$. The vector potential will everywhere remain perpendicular to $\vec{B}$ and not net parallel current will be generated if the velocity distribution functions in the (p_y, p_z) plane are symmetrical with respect to the line corresponding, in the (a_y, a_z) plane, to the vector $\vec{a}_1$.

As we consider transitions for which $\vec{V}_1^{(\nu)} = \vec{V}_2^{(\nu)}$ (Eq. 30), the plasma bulk velocity will vary in direction only when more than two plasma components are present in the layer. In this case the constants $\alpha_i^{(\nu)}$ differ from zero but must satisfy Eqs. 19-20. Taking account of the charge neutrality condition (Eq. 18) it is deduced from Eqs. 19-20 that the constants $\alpha_i^{(\nu)}$ must satisfy the following relation :

$$\sum_{(Z^{(\nu)}, m^{(\nu)})} \alpha_i^{(\nu)} N_i^{(\nu)} = 0 \qquad (37)$$

where the summation is extended to plasma components characterized by the same elementary particles. This kind of transition can be encountered when two hydrogen plasmas are interpenetrated on both sides of the discontinuity. In this case the two populations of electrons (or ions) have generally not the same number densities, temperatures and mean velocities. It is important to note that the perpendicular components of $\vec{V}_i^{(\nu)}$ and $\vec{c}_i^{(\nu)}$ are equal. This is a consequence of Eq. 28. Furthermore, Eq. 30 shows that this perpendicular component is unchanged on both sides of the transition.

From the foregoing it is concluded that $\vec{V}_i^{(\nu)}$, $N_i^{(\nu)}$, $\vec{c}_i$ and $\vec{B}_i$ are not independent quantities but are connected between themselves through Eqs. 18-28-30 and 37. Physically this means that the plasma must be asymptotically charge neutral and uniform. Furthermore, the constancy of the perpendicular components of $\vec{V}_i^{(\nu)}$ is simply the result of the common electric drift imposed to all charged particles. Indeed, when the plasma and fields are uniform, the only perpendicular drift is the electric drift.

3. A MICROSCOPIC DESCRIPTION OF THE MAGNETOPAUSE STRUCTURE

Observations show that the magnetopause is a transition layer through which the magnetic field shifts its direction. In general no significant changes in electron density or energy spectra are observed at the magnetopause (Ref. 12-13). In this section we consider the magnetopause as a current layer in which two hydrogen plasmas are interpenetrated. It is a transition of the type analyzed in section 2.5. We define $i = 1$ ($x = -\infty$) as the magnetosheath side and $i = 2$ ($x = +\infty$) as the magnetospheric side (or more exactly the plasma boundary layer side). The four plasma components are numbered $\nu = 1$ for the solar wind originating electrons, $\nu = 2$ for the magnetosphere originating electrons, $\nu = 3$ for the solar wind originating ions and $\nu = 4$ for the magnetosphere originating ions.

The following typical boundary conditions have been used (for simplicity we consider isotropic temperatures on both sides) : $N_1^{(1)} = N_1^{(3)} = 25\ cm^{-3}$, $N_1^{(2)} = N_1^{(4)} = 1.0379\ cm^{-3}$, $N_2^{(1)} = N_2^{(3)} = 20\ cm^{-3}$, $N_2^{(2)} = N_2^{(4)} = 1\ cm^{-3}$, $T_1^{(1)} = T_2^{(1)} = 5 \times 10^5 K$, $T_{1,2}^{(2)} = 3 \times 10^6 K$, $T_1^{(3)} = T_2^{(3)} = 3 \times 10^6 K$, $T_1^{(4)} = T_2^{(4)} = 4 \times 10^7 K$. For $i = 1$, 2 and $\nu = 1, \ldots, 4$ $V_{y_i}^{(\nu)} = c_{y_i} = 320$ km/s and $V_{z_i}^{(\nu)} = c_{z_i} = 320$ km/s. The initial magnetic induction components are : $B_{y_1} = -35.45$ nT and $B_{z_1} = 6.25$ nT.

We also define $k_1 = 3$, $k_2 = 4$, $k_3 = 1$, $k_4 = 2$ and take the following constants $C_1^{(\nu)}(k_3) = 1$, $C_1^{(\nu)}(k_4) = 1$, $C_2^{(\nu)}(k_3) = 1$, $C_2^{(\nu)}(k_4) = 1$; $\vec{p}_0 = \vec{p}_0 = 0$, for = 1,..., 4. Finally, from Eq. 36, $C_2^{(1)}(k_2) = 1$, $C_2^{(2)}(k_2) = 1$, $C_2^{(3)}(k_2) = 0.77$, $C_2^{(4)}(k_2) = 0.96$.

From these above values of the constant C it can be deduced that the kinetic pressures associated with quadrant E_{k_3} and quadrant E_{k_4} are both larger than the total pressure (kinetic + magnetic) associated with quadrant E_{k_1}. This will allow the extremity of the vector potential to describe a curve ending in the prescribed quadrant E'_{k_2}. Furthermore the layer will neither be an ion layer nor an electron layer but an intermediate layer with electron and ion current components (see the end of section 2.4).

Integration has been started with $a_y^* = -539$ and $a_z^* = -2540$ where $\vec{a}^*$ is a dimensionless vector potential (the vector potential unit is $[m^{(1)} k T_{\#1}^{(1)}]^{1/2}/e$). These initial conditions correspond to a 88° angle between $\vec{a}$ and $\vec{B}$ and have been chosen to produce a rotation $\Delta\theta$ between 90° and 180°. After the integration has been performed a new system of coordinates has been chosen. In this system the direction of the new z axis coincides with the direction of $\vec{B}_2$. In the following part of this section, all the results are given in this new system of coordinates. This system is very useful because in all computations of the magnetopause structure the z axis now coincides with the magnetospheric magnetic induction.

Figure 2 shows the B_y and B_z components of the magnetic induction. On the left hand side a hodogram shows that $\Delta\theta = 136°$. The thickness of this transition is about 200 km. The intensity (B) changes from $B_1 \cong 36$ nT in the magnetosheath to $B_2 \cong 44$ nT in the magnetosphere with a dip at 23 nT near x = 0. A three-dimensional illustration of this magnetic induction variation is also displayed in Figure 3.

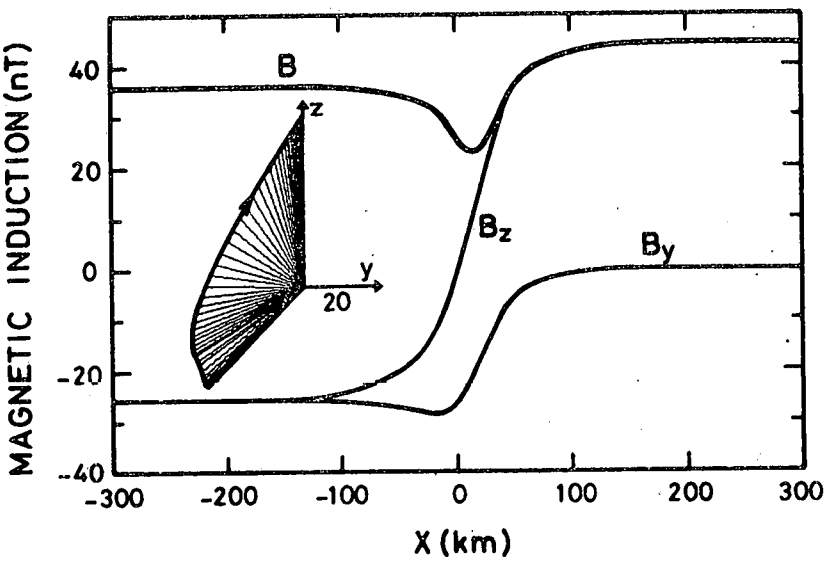

Fig. 2.- Variations of the magnetic induction components (B_y, B_z) and intensity (B) across the magnetopause from the magnetosheath (large negative values of x) to the magnetosphere (large positive values of x). The hodogram on the left hand side shows the magnetic induction has rotated through an angle of 136°. The length of the y axis represents 20 nT. The intensity has a dip at 23 nT near the center of the transition but does not change appreciably on both sides of the magnetopause.

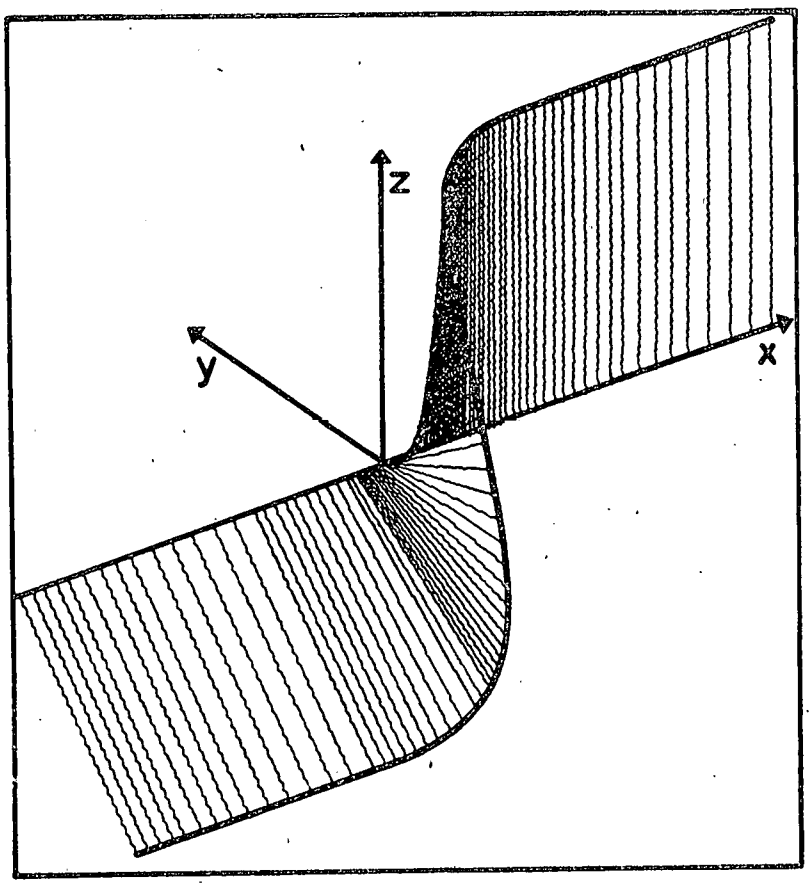

Fig. 3.- A three dimensional representation of the magnetic induction displayed in figure 2 illustrating the spatial variation of the $\vec{B}$ vectors. The length of the x axis represents 1075 km while the lengths of the y and z axes both represents 45 nT.

The current density responsible for the field variation is displayed in Figures 4 and 5. Corresponding hodograms are shown on the left hand sides of these figures. It can be seen that this current is highly field-aligned. The integrated part of this parallel current density is more than twice the integrated part of the perpendicular component. The maximum intensity attains 7.5×10^{-7} A/m^2 at the center of the transition. These field-aligned currents at the magnetopause may constitute a part of the parallel currents observed in the cusps (Ref. 14-15). They can transfer plasma, momentum and energy between the magnetosheath and magnetosphere, or vice versa (Ref. 16).

Figure 6 displays the components (c_y and c_z), the intensity (c) and the parallel ($c_{//}$) and perpendicular ($c_{\perp}$) components of the flow velocity. This bulk velocity is unchanged on both sides (450 km/s) but increases at the center ($\sim$ 600 km/s) while changing slightly its orientation as shown by, the hodogram on the left hand side. In the magnetosphere the bulk velocity is highly field-aligned ($c_{//2}$) = 444 km/s) with a small perpendicular component ($c_{\perp 2}$ = - 88 km/s).

Electric field (E), electrical potential (ϕ) and charge separation ($\Delta n/n$) are illustrated in Figure 7. The potential ϕ is deduced from the charge neutrality approximation given by Eq. 10. The asymptotic values of the electric field correspond to the convection electric field due to the plasma motion across the field lines. As the magnetic field direction is nearly reversed while the flow velocity keeps the same orientation on both sides of the transition, this electric field changes sign when passing through $x = 0$. In the magnetosheath, the bulk velocity has a significant perpendicular component (see Figure 6) and produces a convection electric field of - 13 mV/m. However, the bulk velocity in the magnetosphere is nearly field-aligned (see Figure 6) and produces a convection electric field of only + 3 mV/m. The charge separation displayed in the bottom panel of Figure 7 is everywhere negligible, being everywhere less than 6×10^{-7}. This supports a priori

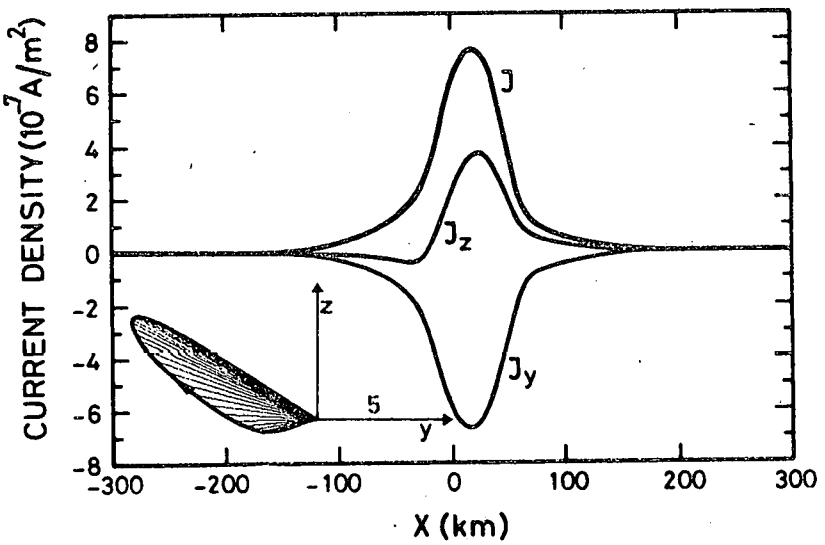

Fig. 4.- Intensity (J), y component (J_y) and z component (J_z) of the total current density across the magnetopause. The maximum intensity attains 7.5×10^{-7} A/m^2 near the center of the transition. A corresponding hodogram is shown in the left corner of this figure. Its y axis represents 5×10^{-7} A/m^2. This current density produces the magnetic induction variation displayed in figures 2 and 3.

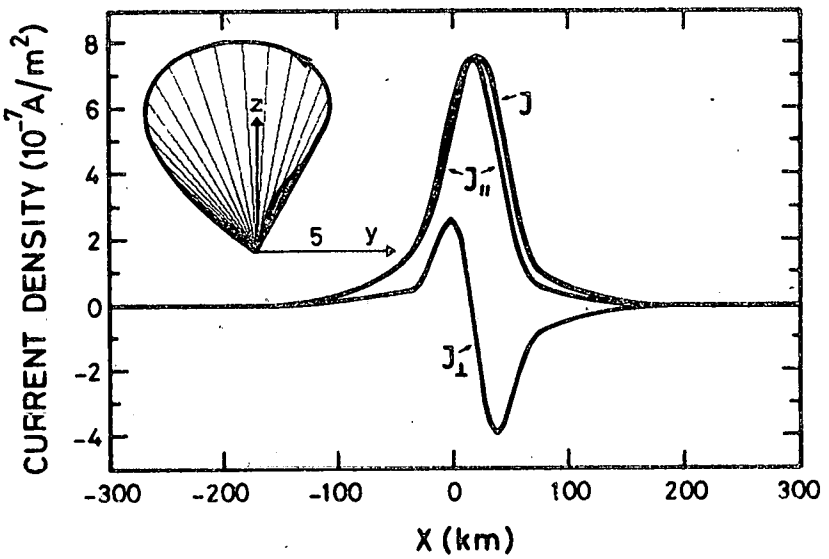

Fig. 5.- The current density displayed in figure 4 is represented in this figure by its parallel ($J_{\parallel}$) and perpendicular ($J_{\perp}$) components. The J curve still represents the corresponding vector intensity. The hodogram in the left upper corner refers to a local frame of reference whose z axis is orientated along the local $\vec{B}$ induction. $J_{\perp}$ has the same orientation as the local y axis so that x, $J_{\perp}$ and $J_{\parallel}$ form a right-hand system. The length of the y axis represents 5×10^{-7} A/m^2. The current density at the magnetopause is highly field-aligned since $J_{\parallel}$ is everywhere larger than $J_{\perp}$.

the charge neutrality approximation (Eq. 10) used for solving Poisson equation (Eq. 3).

Figures 8 and 9 illustrate the number densities and mean temperatures variations across the transition. The number densities $n^{\mp}_{sw}$ represent the electron (-) or ion (+) number densities from solar wind (sw) origin for which $\nu = 1$ (electrons) or $\nu = 3$ (ions). In the same way $n^{\mp}_{m}$ are the number densities from magnetospheric (m) origin for which $\nu = 2$ (electrons) or $\nu = 4$ (ions). A similar notation is used for the temperatures on both sides. In Figure 9, $< T^{+} >$ and $< T^{-} >$ are the mean temperatures of ions and electrons defined by

$$< T^{\pm} > = (n^{\pm}_{sw}\ \tau^{\pm}_{sw} + n^{\pm}_{m}\ \tau^{\pm}_{m})/(n^{\pm}_{sw} + n^{\pm}_{m}) \qquad (38)$$

where τ are the temperatures across the transition.

It can be seen that the densities have a peak near $x = 0$ but their variations are not important. It is interesting to note that ions and electrons from the same origin have not exactly the same concentrations although the plasma remains locally charge neutral. The temperatures displayed in Figure 9 exhibit small amplitude variations but have a tendency to increase when going from the magnetosheath to the magnetosphere.

4. A MICROSCOPIC DESCRIPTION OF THE INNER EDGE OF THE PLASMA BOUNDARY LAYER

The plasma boundary layer (Ref. 17 to 21) is a region of magnetosheath-like plasma located immediately earthward of the magnetopause layer. This layer is located inside the magnetosphere. Its thickness is generally much larger than the thickness of the magneto-

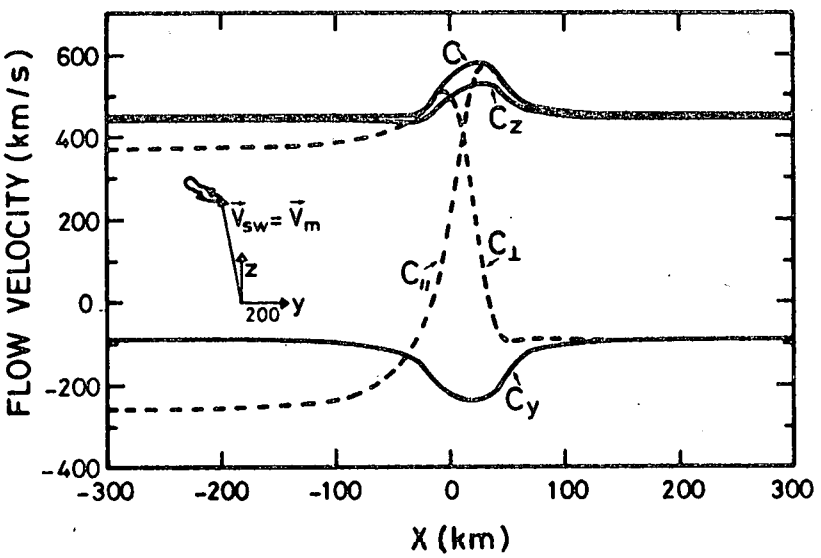

Fig. 6.- Intensity (c), y component (c_y) and z component (c_z) of the flow velocity across the magnetopause. The dotted curves represent the parallel ($c_\parallel$) and perpendicular ($c_\perp$) components of this flow velocity. The hodogram displayed on the left hand side of this figure shows that the flow velocity changes slightly its orientation near x = 0 where the intensity (c) attains a maximum value of nearly 600 km/s. However, this flow velocity remains unchanged on both sides of the magnetopause current layer where the mean velocities of the plasma constituents are all equal to the flow velocity, i.e., $\vec{c}_{sw} = \vec{c}_m = \vec{V}^{(\nu)}_{sw} = \vec{V}^{(\nu)}_m$. The length of the y axis represents 200 km/s. Because of the large $\vec{B}$ rotation displayed in figures 2 and 3, the parallel ($c_\parallel$) and perpendicular ($c_\perp$) components, exhibit significant variations. In the magnetosphere (x = + ∞), the flow becomes highly field-aligned ($c_{\parallel 2}$ = 444 km/s) with a small perpendicular component ($c_{\perp 2}$ = - 88 km/s).

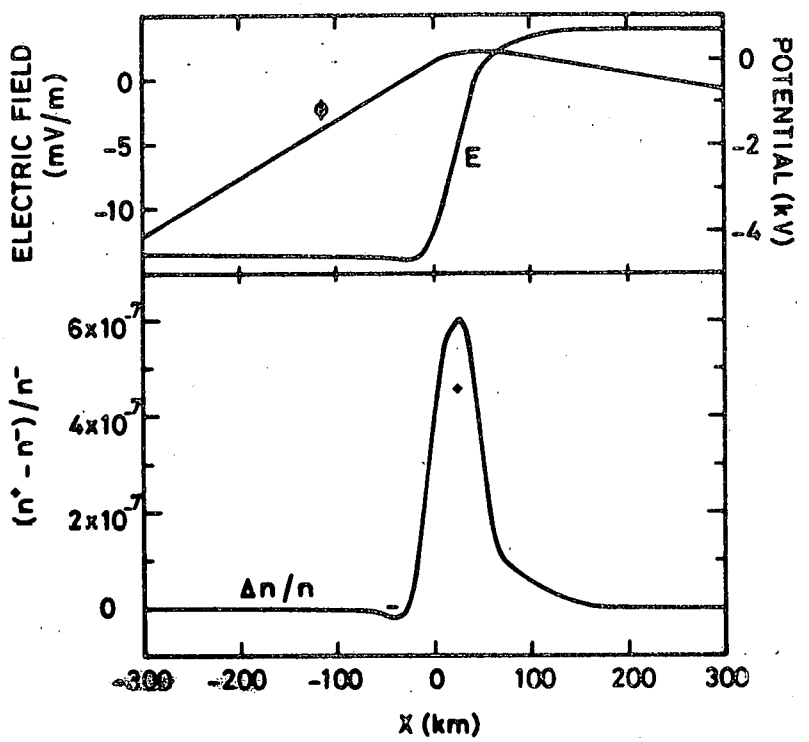

Fig. 7.- Electrical potential (ϕ) and electric field (E) across the magnetopause are displayed in the upper panel of this figure. The potential ϕ is deduced from the charge neutrality condition. The electric field is normal to the plane of the discontinuity. As a consequence of plasma motion across field lines this electric field on both sides becomes a convection electric field. The relative charge separation ($\Delta n/n$) is shown in the lower panel. Here n^+ is the total ion number density ($n^{(3)} + n^{(4)}$) and n^- is the total electron number density ($n^{(1)} + n^{(2)}$).

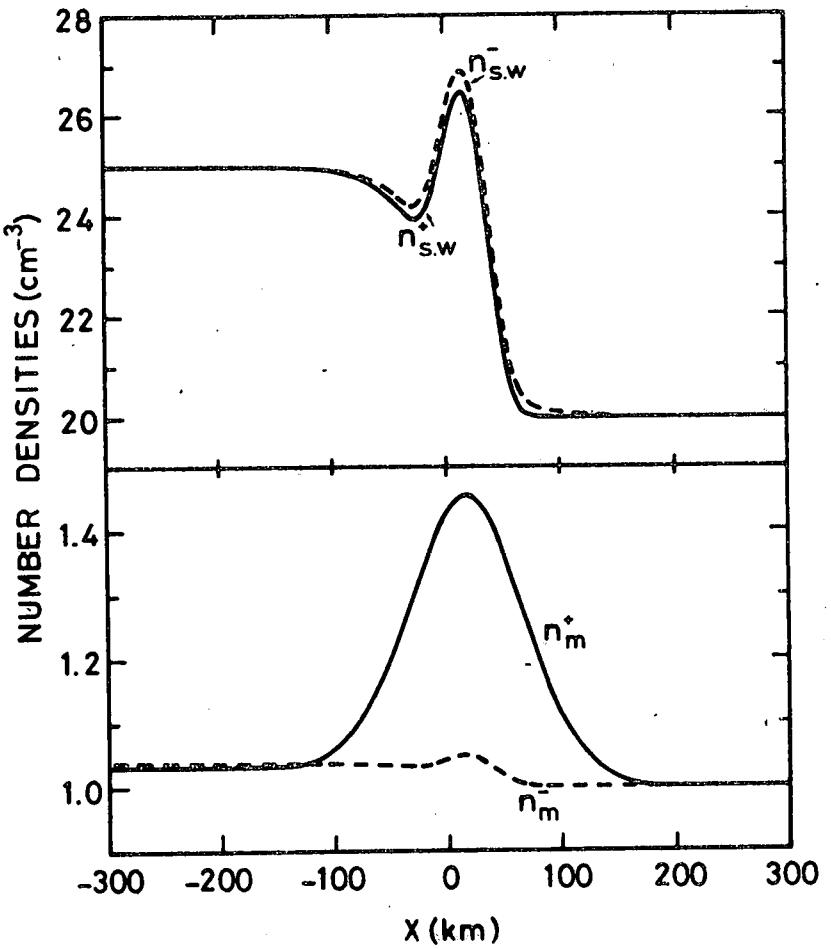

Fig. 8.- Number densities across the magnetopause. In the upper panel, n^+_{sw} and n^-_{sw} are respectively the ion ($\nu = 3$) and electron ($\nu = 1$) number densities of solar wind origin. In the lower panel, n^+_m and n^-_m are respectively the ion ($\nu = 4$) and electron ($\nu = 2$) number densities of magnetospheric origin. It can be seen that ions and electrons from the same origin have not exactly the same concentrations, although the plasma remains locally quasi-neutral.

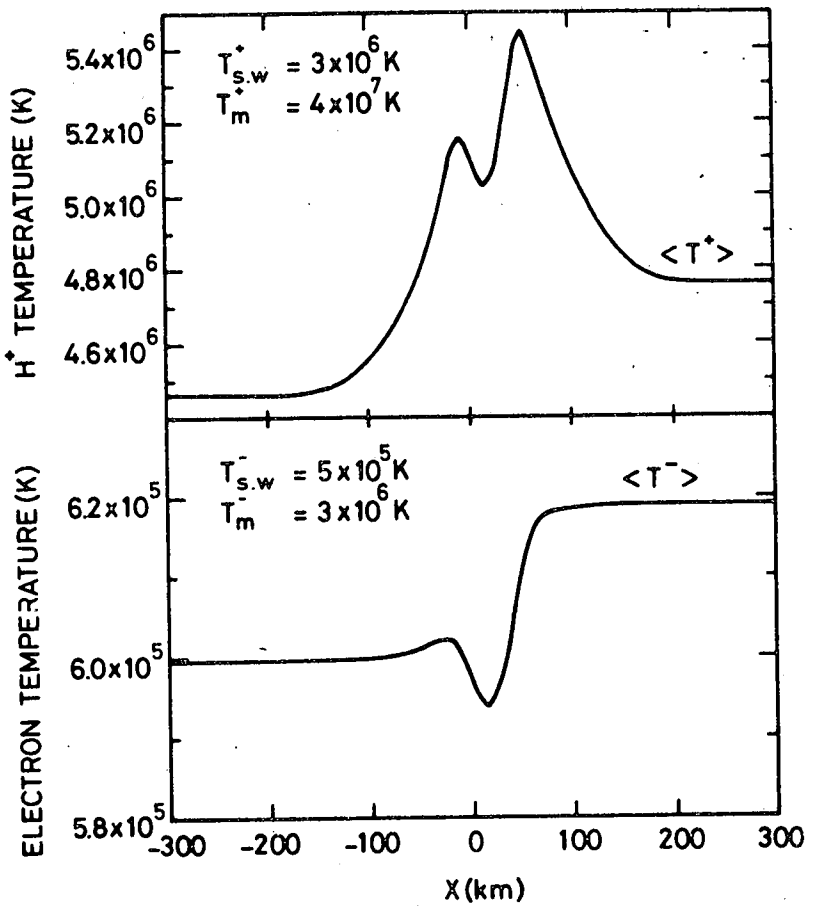

Fig. 9.- Mean ion and electron temperatures are respectively displayed in the upper and lower panels as a function of the distance normal to the magnetopause. The temperatures of the different plasma components are unchanged on both sides of the transition and their values are recalled in the left upper corner of each panel. In the upper panel T^+_{sw} and T^-_{sw} are respectively the asymptotic ion ($\nu = 3$; $i = 1, 2$) and electron ($\nu = 1$; $i = 1, 2$) temperatures of the solar wind particles. In the lower panel T^+_m and T^-_m are respectively the asymptotic ion ($\nu = 4$; $i = 1, 2$) and electron ($\nu = 2$; $i = 1,2$) temperatures of the magnetospheric particles.

pause layer. At its inner edge, towards the Earth, variations in bulk velocity and plasma parameters are often observed while the direction of the magnetic induction remains unchanged. This inner edge constitutes a transition of the type analyzed in section 2.6. Here i = 1 defines the plasma boundary layer side ($x = -\infty$) and i = 2 denotes the magnetosphere side ($x = +\infty$). The four plasma components are numbered as in section 3.

With isotropic temperatures the following typical boundary conditions have been used : $N_1^{(1)} = N_1^{(3)} = 10\ cm^{-3}$, $N_1^{(2)} = N_1^{(4)} = 1\ cm^{-3}$, $N_2^{(1)} = N_2^{(3)} = 1.5\ cm^{-3}$, $N_2^{(2)} = N_2^{(4)} = 0.7289\ cm^{-3}$, $T_1^{(1)} = T_2^{(1)} = 5 \times 10^5$ K, $T_1^{(2)} = T_2^{(2)} = T_1^{(3)} = T_2^{(3)} = 3 \times 10^6$K, $T_1^{(4)} = T_2^{(4)} = 4 \times 10^7$K. For $\nu = 1, \ldots, 4$ $V_y^{(\nu)} = V_y^{(\nu)} = c_{y_1} = c_{y_2} = 17$ km/s while $V_{z_1}^{(1)} = V_{z_2}^{(1)} = 189.277$ km/s, $V_{z_1}^{(2)} = V_{z_2}^{(2)} = -308.744$ km/s, $V_{z_1}^{(3)} = V_{z_2}^{(3)} = 189.277$ km/s, $V_{z_1}^{(4)} = V_{z_2}^{(4)} = -308.774$ km/s, $c_{z_1} = 144$ km/s, $c_{z_2} = 26.4$ km/s. The magnetic induction components are $B_{y_1} = 0$ nT and $B_{z_1} = 80$ nT. We also define $k_1 = 1$, $k_2 = 2$, $k_3 = 3$, $k_4 = 4$ and adopt the constants $C_1^{(\nu)}(k_3) = 1$, $C_1^{(\nu)}(k_4) = 0$, $C_2^{(\nu)}(k_3) = 0$, $C_2^{(\nu)}(k_4) = 1$; $\vec{p}_{0_1}^{(\nu)} = \vec{p}_{0_2}^{(\nu)} = 0$, for $\nu = 1, \ldots, 4$. Finally, from Eq. 36, $C_2^{(1)}(k_2) = 1$, $C_2^{(2)}(k_2) = 1$, $C_2^{(3)}(k_2) = 0.109$, $C_2^{(4)}(k_2) = 0.712$. The integration has been started with $a_y^* = -1500$ and $a_z^* = 0$, i.e., with $\vec{a}.\vec{B} = 0$. These above conditions have been chosen to satisfy Eqs. 18-28-30 and 37. No rotation of the magnetic induction is allowed for since the velocity distribution functions are symmetrical with respect to the p_y axis. Furthermore, the above temperatures and values of constants $C_i^{(\nu)}(k_3)$, $C_i^{(\nu)}(k_4)$ and $C_2^{(\nu)}(k_2)$ for $\nu = 1, 2$ indicate that we have an ion layer as described in the last paragraph of section 2.4.

Figure 10 is an illustration of the bulk velocity variation. A small perpendicular component ($c_y = 17$ km/s) is applied on both sides of the transition while a substantial parallel component ($c_{z_1} = 144$ km/s) is allowed for on the plasma boundary layer side.

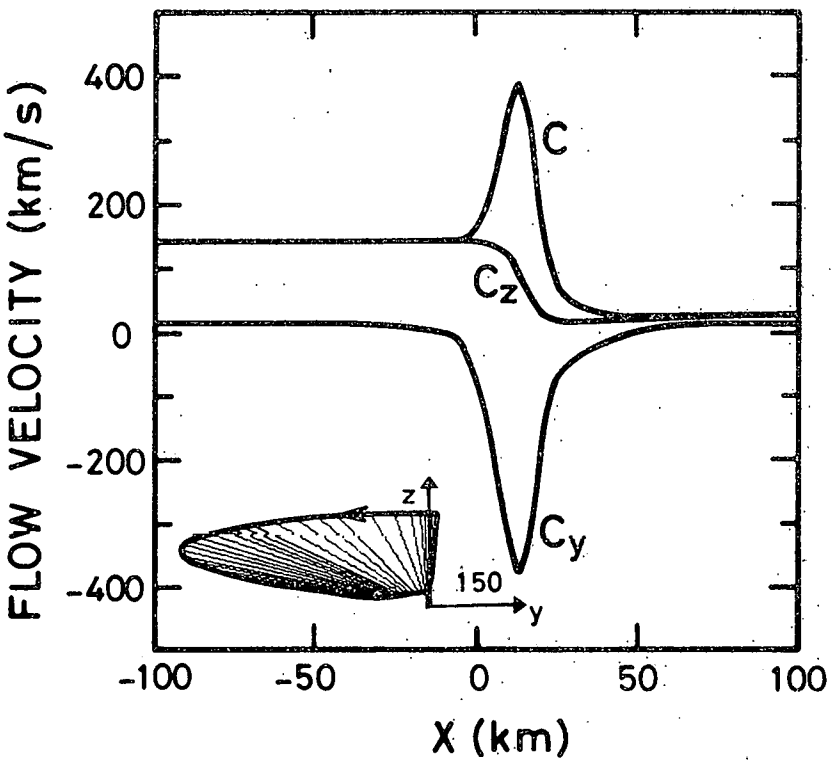

Fig. 10.- Intensity (c), y component (c_y) and z component (c_z) of the flow velocity across the inner edge of the plasma boundary layer from the plasma boundary layer (large negative values of x) to the magnetosphere (large positive values of x). The hodogram in the left lower corner shows that the flow velocity has rotated through an angle of more than 180°. The length of the y axis represents 150 km/s. The parallel component (c_z) decreases monotonously from 144 km/s to 26.4 km/s, while the perpendicular component has a peak of nearly 400 km/s near x = 0 due to the intense ion current density. All the plasma components have the same asymptotic perpendicular mean velocities equal to 17 km/s.

Across the transition the parallel component decreases monotonously while the perpendicular component has a peak of nearly 400 km/s near x = 0. The hodogram displayed on the left hand side of Figure 10 shows that the rotation of the bulk velocity is larger than 180°. This variation of the bulk velocity is also represented in three-dimensions in Figure 11.

The peak in the perpendicular velocity is due to the displacement of ions from their mean positions in a frame of reference with the bulk velocity of electrons. This ion displacement across the field lines generate the current density. As the number density jump from one side to the other is relatively important in this example, it is reasonable that the current density and the perpendicular bulk velocity become intense. This is rarely observed in the plasma boundary layer but this could happen at the inner edge when the density jump becomes sharp as assumed in this example.

The magnetic induction (B_z) and current density (J_y) are displayed in Figure 12. These two vectors are perpendicular and no field-aligned current can be generated. The amplitude of the magnetic induction variation is relatively small ($\cong$ 8 nT) and the peak current intensity attains 3.5×10^{-7} A/m^2. The thickness of the transition is about 100 km which represents half of the magnetopause thickness evaluated in section 3. Electric field (E), electrical potential (ϕ) and charge separation ($\Delta n/n$) are illustrated in Figure 13. On both sides the electric field is negative and equal to the convection electric field $\vec{c} \wedge \vec{B}$. In the center of the transition the electric field has a positive peak of 4 mV/m due to the charge separation displayed in the bottom panel of Figure 13. This charge separation ($\Delta n/n$) remains quite small and less than 1.25×10^{-5}.

Finally, figures 14 and 15 show the number densities and the mean temperatures as given by Eq. 38. The notations are similar to

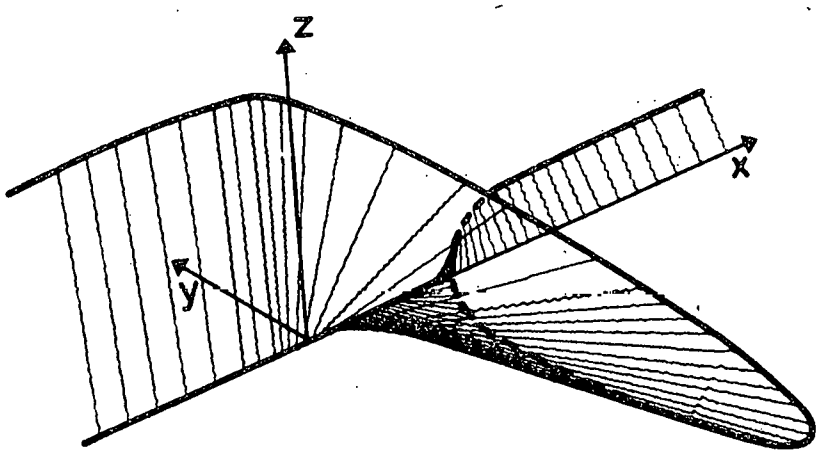

Fig. 11.- A three-dimensional representation of the flow velocity displayed in figure 10, illustrating the spatial variation of the $\vec{c}$ vectors. The length of the x axis represents 205 km, while the lengths of the y and z axes represent respectively 125 km/s and 175 km/s.

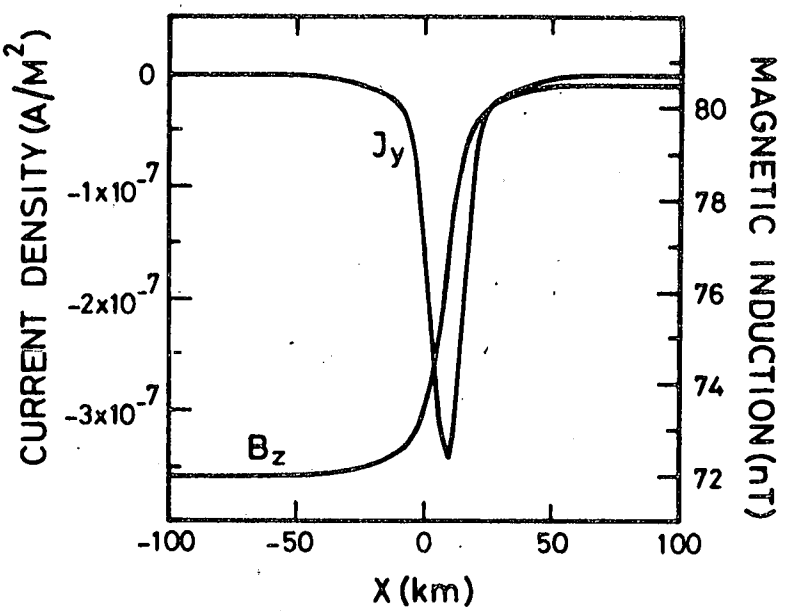

Fig. 12.- Total current density (J_y) and magnetic induction (B_z) variations across the inner edge of the plasma boundary layer. The magnetic induction remains aligned along the z axis while the total current density is always oriented along the y axis, i.e., $\vec{J}.\vec{B} = 0$ and there is no field-aligned current.

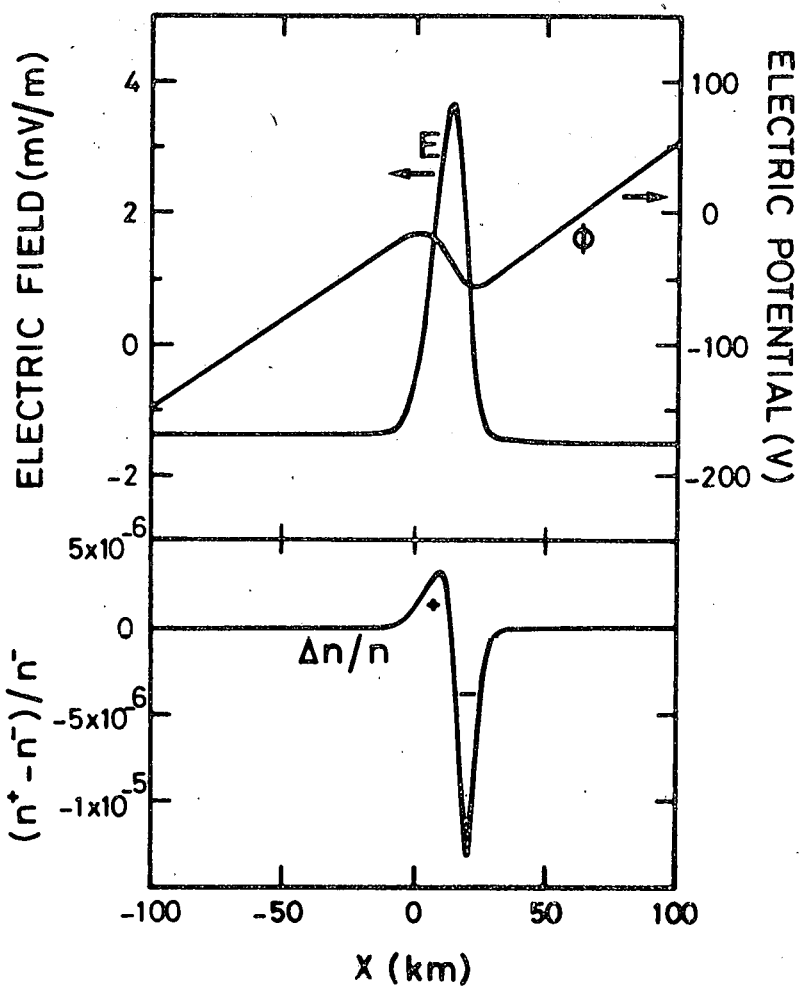

Fig. 13.- Electrical potential (ϕ) and electric field (E) across the inner edge of the plasma boundary layer are displayed in the upper panel of this figure. The potential ϕ is deduced from the charge neutrality condition. The electric field is normal to the plane of the discontinuity. As a consequence of charge separation into the layer, a peak electric field is set up near the center of the transition. Its intensity grows up to nearly 4 mV/m. The relative charge separation ($\Delta n/n$) is shown in the lower panel. Here n^+ is the total ion number density ($n^{(3)} + n^{(4)}$) and n^- is the total electron number density ($n^{(1)} + n^{(2)}$).

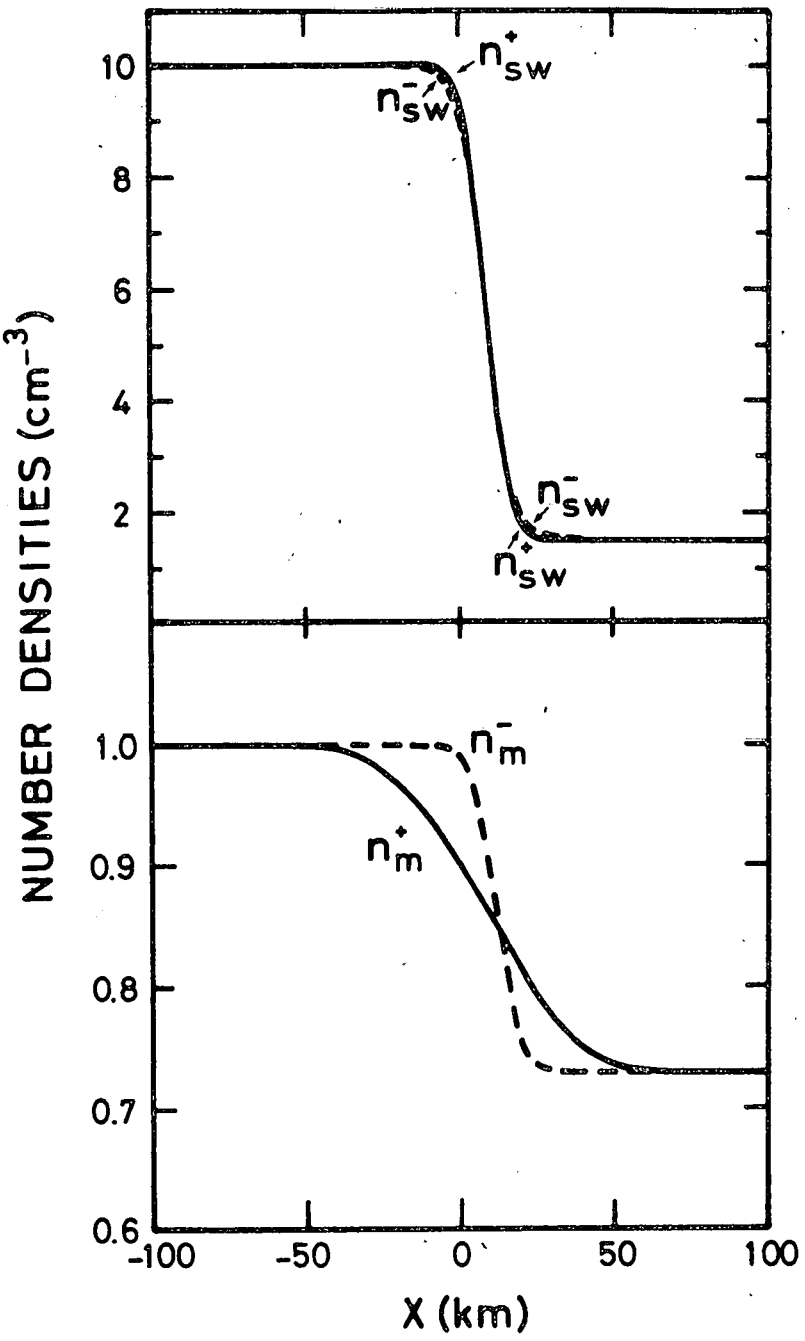

Fig. 14.- Number densities across the inner edge of the plasma boundary layer. In the upper panel, n^+_{sw} and n^-_{sw} represent respectively the ion (ν = 3) and electron (ν = 1) number densities of solar wind origin. In the lower panel, n^+_m and n^-_m represent respectively the ion (ν = 4) and electron (ν = 2) number densities of magnetospheric origin. It can be seen that ions and electrons from the same origin have not exactly the same concentrations, although the plasma remains locally quasi-neutral.

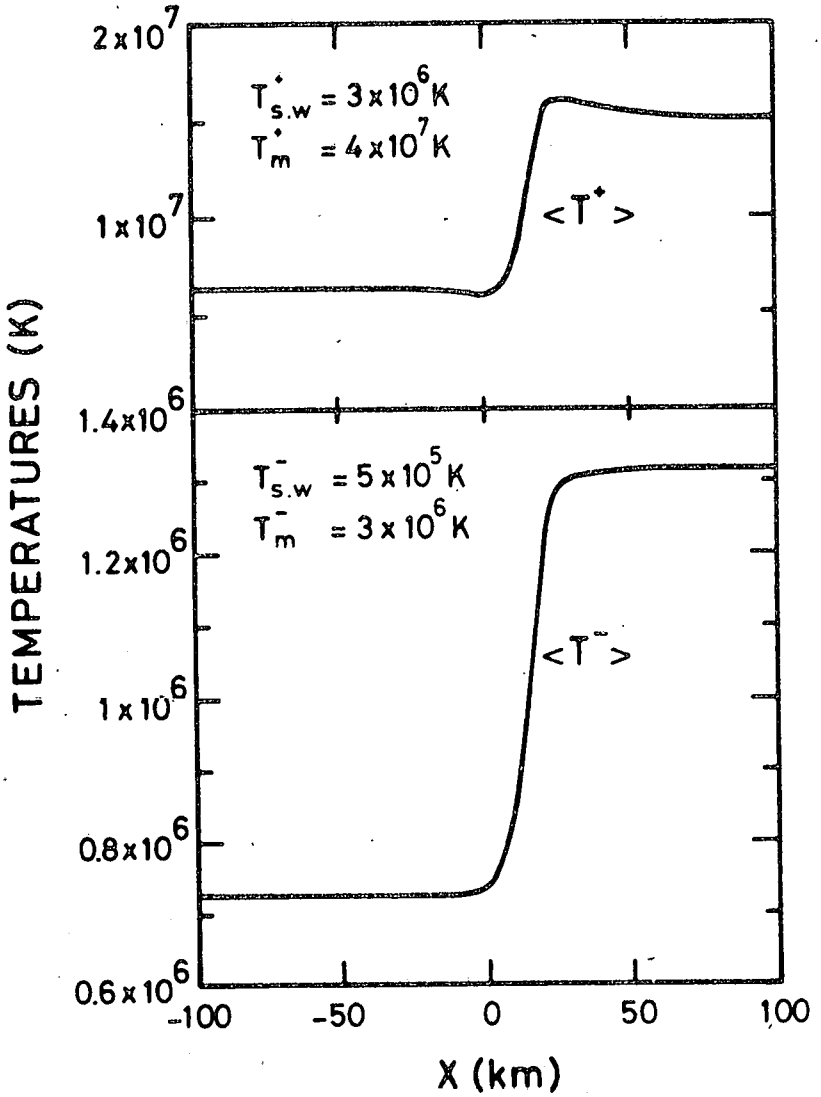

Fig. 15.- Mean ion and electron temperatures are respectively displayed in the upper and lower panels as a function of the distance normal to the inner edge of the plasma boundary layer. The temperatures of the different plasma constituents are unchanged on both sides of the transition and their values are recalled in the left upper corner of each panel. In the upper panel T^{+}_{sw} and T^{-}_{sw} are respectively the asymptotic ion ($\nu = 3$; $i = 1, 2$) and electron ($\nu = 1$; $i = 1, 2$) temperatures of the solar wind particles. In the lower panel T^{+}_{m} and T^{-}_{m} are respectively the asymptotic ion ($\nu = 4$; $i = 1, 2$) and electron (; 2; $i = 1,2$) temperatures of the magnetospheric particles.

those of Figures 8 and 9 displayed in section 3. It can be seen that the number densities decrease monotonously towards the magnetosphere interior while the reverse variation is seen in the temperature profiles. In fact, these types of variation are characteristic of the low latitude plasma boundary layer (Ref. 12-13).

5. STABILITY AND THICKNESS OF A VLASOV-MAXWELL TANGENTIAL DISCONTINUITY

The stability of structures analyzed in this paper represents a difficult problem. Nevertheless (Ref. 11) some results have been found in the special case of a two components hydrogen plasma whose current carriers are either the electrons or the ions. (The so-called electron layers or ion layers in Sestero theory, Ref. 2). In such layers the temperatures and mean velocities of the two plasma constituents are unchanged on both sides of the transition. In this section we shall summarize the principal results.

Figures 16 and 17 illustrate the stability of electron and ion layers with respect to ordinary (O) and modified (M) two-stream instabilities (Ref. 22). Curves labeled (O) and (M) are the locations in the (u, n_2) plane where the threshold for instability is attained somewhere in the transition. The absciss u represents the temperature ratio T^+/T^- while the ordinate n_2 represents the asymptotic number density ratio N_2/N_1. (It is assumed that the value of the number density is the largest on side 1). For the two-stream instabilities the shaded areas represent the stable domains of the (u, n_2) plane. From Figure 16, it can be seen that the electron layers are nearly always unstable with respect to the modified two-stream instability. Indeed, these layers can only support a very small density variation when the temperature ratio is not too different from unity.

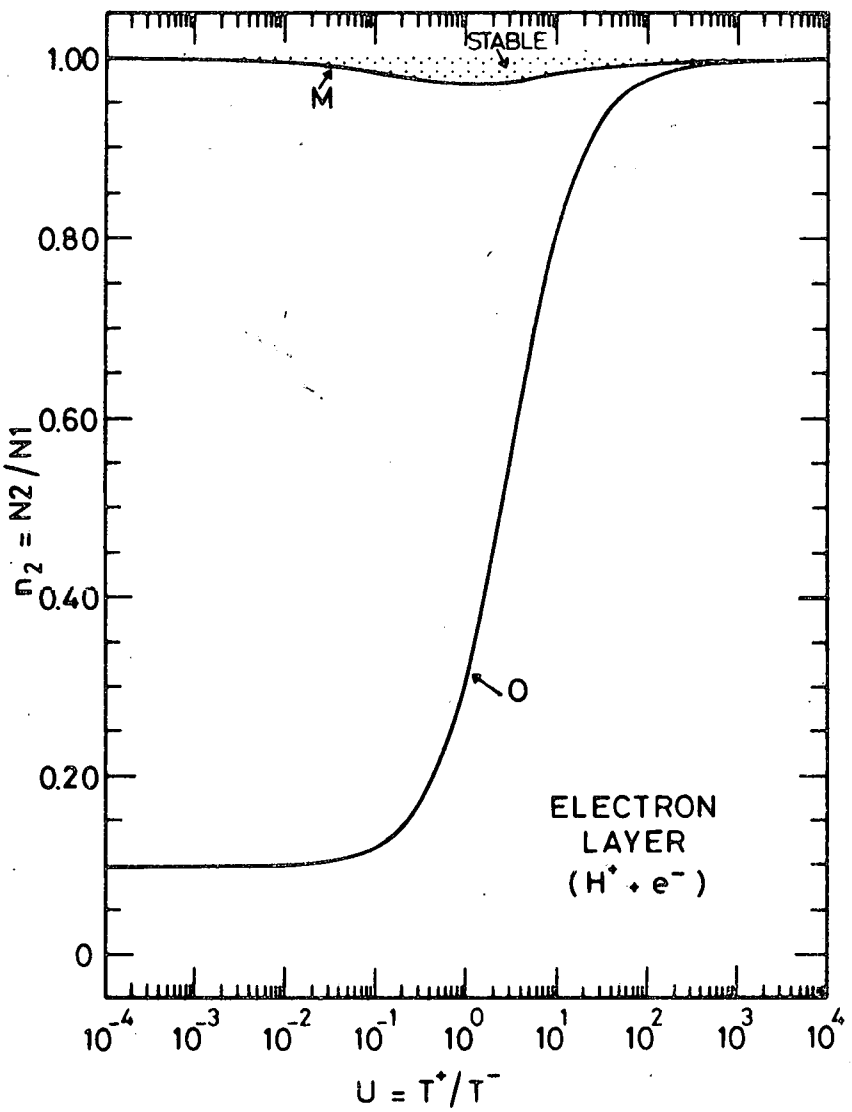

Fig. 16.- Stability of an electron layer with respect to the ordinary (O) and modified (M) two-stream instabilities. The curves are the locations in the (u, n_2) plane where the threshold for instability is attained somewhere into the transition. Shaded area shows the stable domain of the (u, n_2) plane.

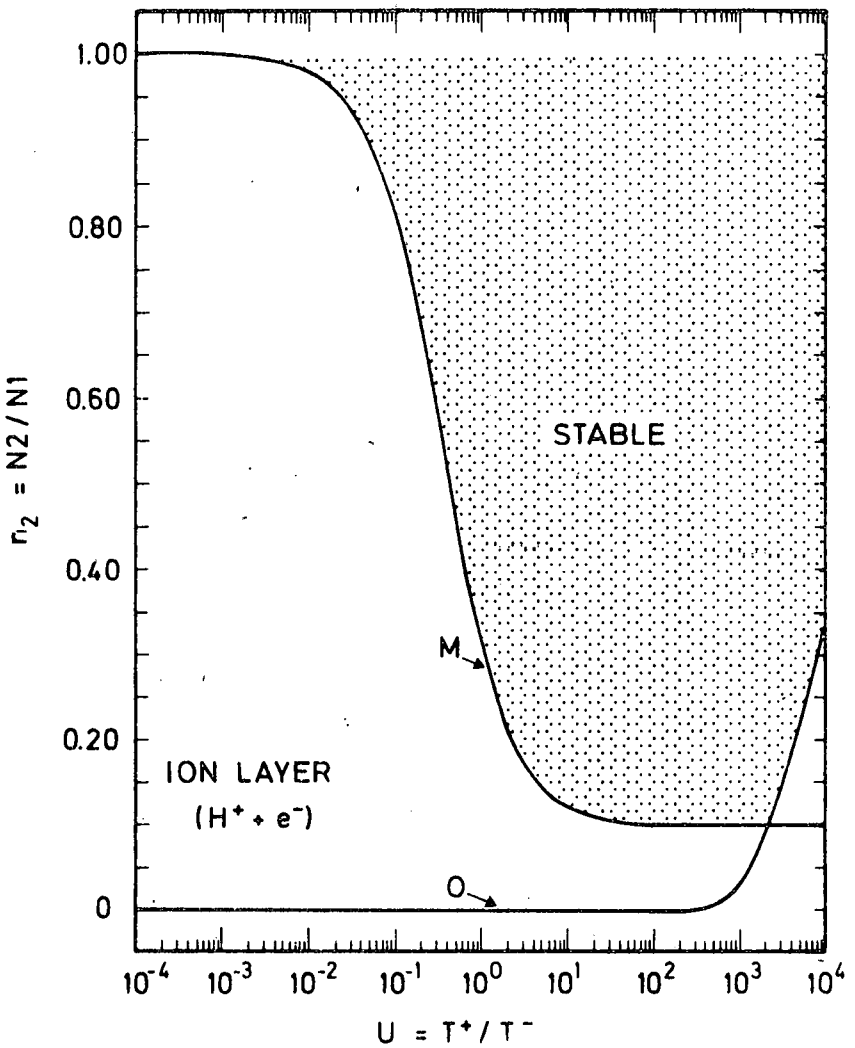

Fig. 17.- Stability of an ion layer with respect to ordinary (O) and modified (M) two-stream instabilities. The curves are the locations in the (u, n_2) plane where the threshold for instability is attained somewhere into the transition. Shaded area shows the stable domain of the (u, n_2) plane.

However ion layers can be stable in a large fraction of the (u, n_2) plane as shown in Figure 17. At the magnetopause, $u = 10$ (Ref. 13) and the maximum allowed variation of the number density is 90% (i.e., $n_2 = 0.1$) for an ion layer. Larger variations would make these transitions unstable with respect to the modified two-stream instability.

A definition of the transition thickness is given by Figure 18 for a monotonously decreasing density. For ion layers this thickness is shown in Figure 19 in unit of the ion gyro-radius measured at the center of the transition. It is given as a function of the ratio u. The value of β_1^- (ratio of the electron kinetic pressure to the magnetic pressure on side 1) has been assumed equal to 1.5. It can be seen from Figure 19 that for $u > 5$, the thickness tends to become equal to 2.5 ion gyro-radii whatever the value of n_2 (> 0.1) may be. The absolute value of the ion layer thickness is displayed in Figure 20. The unit is now the electron inertial length (Ref. 23 to 26) which is inversely proportional to the square root of the electron density on side 1. For a typical magnetosheath density of 10 cm^{-3} this unit represents 1 km, i.e., the classical Ferraro magnetopause thickness (Ref. 23). Figure 20 shows that the measured thickness of an ion layer increases with u. For u values larger than 1 the thickness is also increasing with n_2. But for u smaller than 0.1 the thickness is decreasing when n_2 is increasing.

For $u = 10$ the magnetopause thickness is expected to be about 100 km ($N_1 \cong 10$ cm^{-3}) for $n_2 = 0.2$. But this thickness increases substantially when the density variation decreases (i.e., when $n_2 \to 1$).

These results explain pretty well why the magnetopause is rarely observed with thickness smaller than 100 km. The minimum magnetopause thickness is therefore close to the Parker magnetopause thickness (Ref. 27) rather than close to the Ferraro magnetopause thickness.

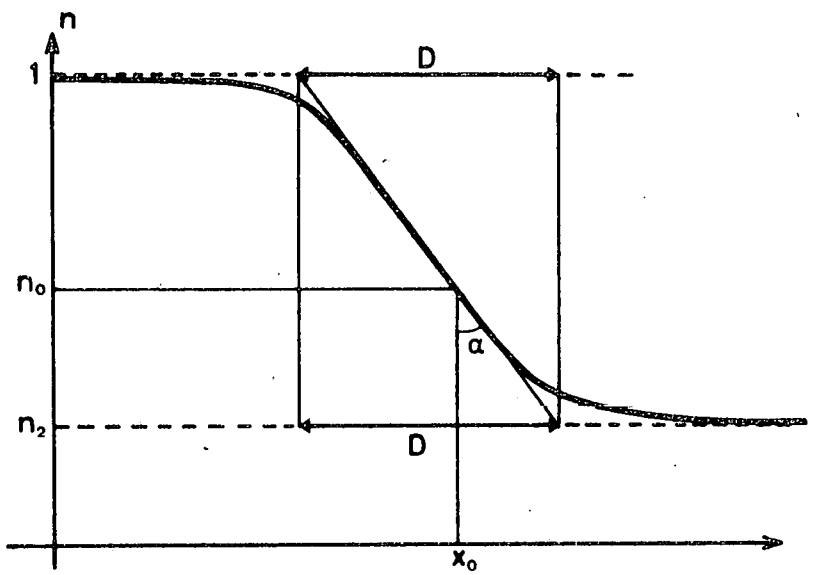

Fig. 18.- Definition of the transition thickness D. The number density normalized to unity at $x = -\infty$ is assumed to decrease monotonously towards n_2 at $x = +\infty$. The thickness (D) is between the points of intersection of the tangent to the slope at the point of inflexion with lines parallel to the asymptotic densities.

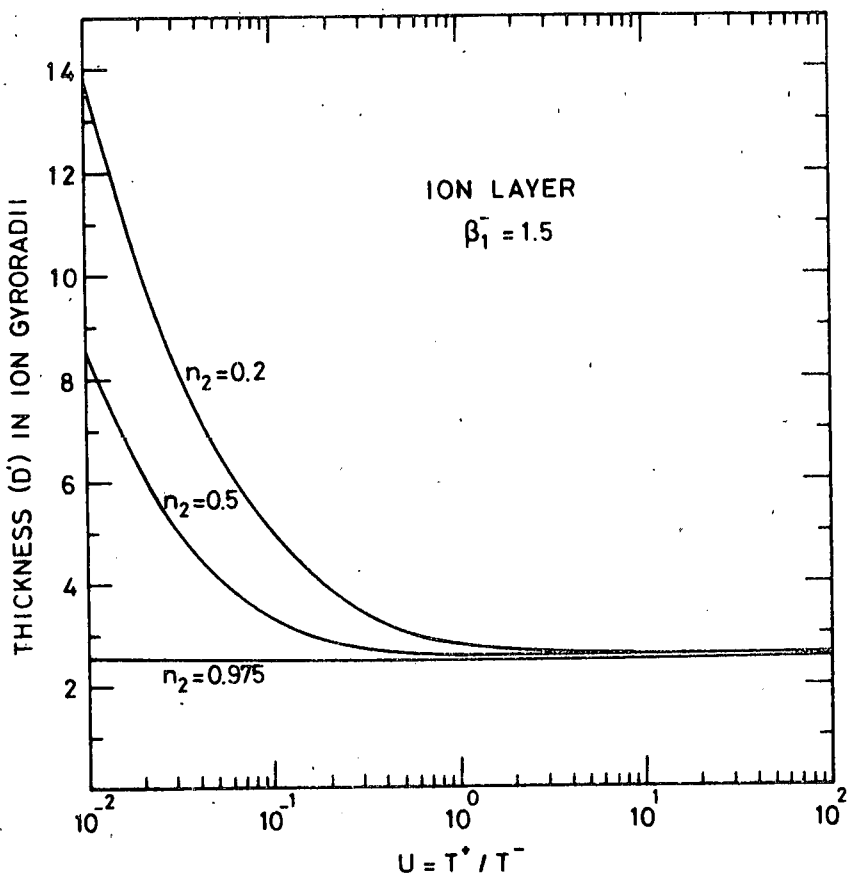

Fig. 19.- Thickness of an ion layer in unit of the ion gyroradius as a function of the temperature ratio T^+/T^- for different values of the density ratio N_2/N_1 when $\beta_1^- = 1.5$.

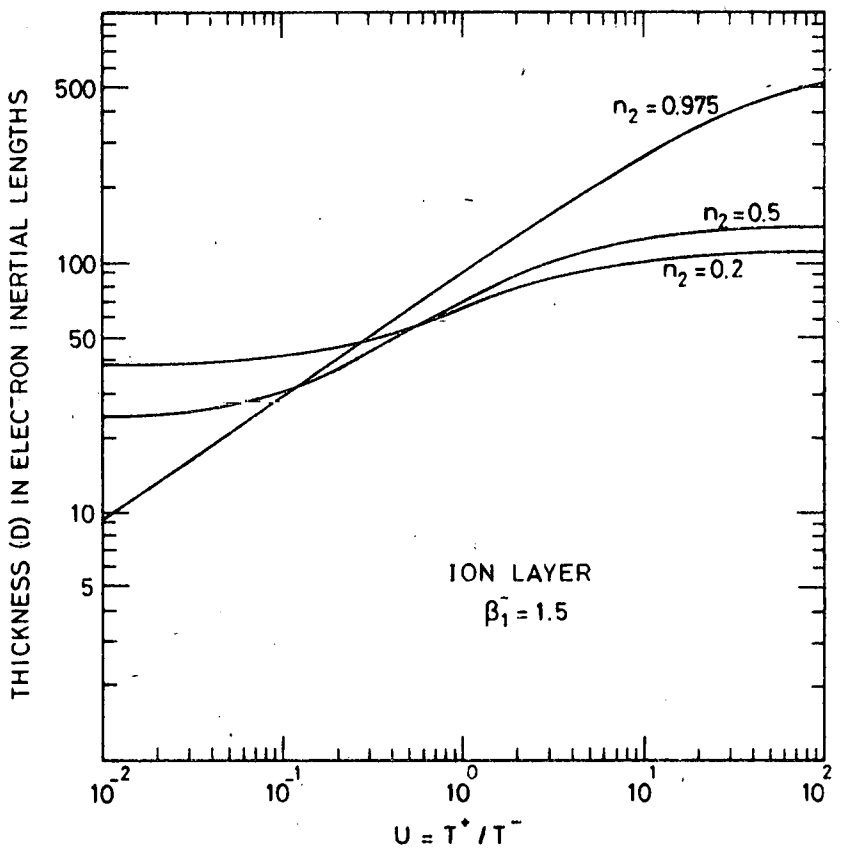

Fig. 20.- Thickness of an ion layer in unit of the electron inertial length as a function of the temperature ratio T^+/T^- for different values of the density ratio N_2/N_1 when $\beta_1^- = 1.5$.

6. CONCLUSIONS

The kinetic model of tangential discontinuities described in this paper has been used to represent the magnetopause and inner edge of the plasma boundary layer. In the former case, the magnetic induction changes orientation in an arbitrary way while the bulk velocity remains unchanged on both sides. In the latter case, the plasma bulk velocity is able to vary both in intensity and direction while the magnetic induction remains oriented along a given direction. The variation of the plasma bulk velocity is made compatible with the presence of different convection electric fields on both sides of the transition.

At the magnetopause high field-aligned currents can be generated. These parallel currents may constitute a part of the field-aligned currents observed in the cusps and can transfer plasma, momentum and energy between the magnetosheath and magnetosphere.

Ordinary and modified two-stream instabilities play an important role on the microstability of the current sheets analyzed in this paper. It has been shown that for a hydrogen plasma, electron layers are nearly always unstable, but ion layers can be stable for conditions pertaining to the magnetopause or to the plasma boundary layer (i.e., $u = T^+/T^- \cong 10$, $n_2 = N_2/N_1 > 0.1$). It is also shown that the thickness of these ion layers are at least equal to 2.5 ion gyro-radii evaluated at the center of the transition. However, the absolute thickness increases when the ratio T^+/T^- increases and/or when the density variation decreases.

For the magnetopause ($u = 10$), we have deduced a minimum thickness of 100 km. This minimum thickness is attained when the density variation through the sheath becomes equal to 80% ($n_2 = 0.2$), i.e., when the density ratio N_2/N_1 becomes close to the threshold value for the modified two-stream instability.

REFERENCES

1. FALTHAMMAR, G.G. et al. 1978, The significance of magnetospheric research for progress in astrophysics, Nature vol 275 (5677), 185-188.
2. SESTERO, A. 1964, Structure of plasma sheaths, Phys. Fluids 7 (1), 44-51.
3. SESTERO, A. 1966, Vlasov equation study of plasma motion across magnetic fields, Phys. Fluids 9 (10), 2006-2013.
4. ALPERS, W. 1969, Steady state charge neutral models of the magnetopause, Astrophys. Space Sci. 5 (2), 425-437.
5. KAN, J.R. 1972, Equilibrium configurations of Vlasov plasmas carrying a current component along a external magnetic field, J. Plasma Phys. 7 (3), 445-459.
6. ROTH, M. 1976, The plasmapause as a plasma sheath : a minimum thickness, J. Atmo. Terr. Phys. 38 (11), 1065-1070.
7. LEMAIRE, J. and L.F. BURLAGA 1976, Diamagnetic boundary layers : a kinetic theory, Astrophys. Space Sci. 45 (2), 303-325.
8. ROTH, M. 1978, Structure of tangential discontinuities at the magnetopause : the nose of the magnetopause, J. Atmo. Terr. Phys. 40 (3), 323-329.
9. LEE, L.C. and J.R. KAN 1979, A kinetic model of the magnetopause, submitted to J. Geophys. Res.
10. RALSTON, A. and H.S. WILF 1965, Mathematical methods for digital computers, John Wiley and Sons, New-York 293 p.
11. ROTH, M. 1979 Structure interne de la magnétopause, Ph. D. Thesis (in preparation).
12. EASTMAN, T.E. and E.W. Jr. HONES 1979, Characteristics of the Magnetospheric Boundary Layer and Magnetopause Layer as Observed by Imp6, J. Geophys. Res. 84 (A5), 2019-2028.

13. EASTMAN, T.E. 1979, The plasma boundary layer and magnetopause layer of the Earth's magnetosphere, Ph. D. Thesis, The University of Alaska, Fairbanks.

14. IIJIMA, T. and T.A. POTEMRA 1976, Field-Aligned Currents in the Dayside Cusp Observed by Triad, J. Geophys. Res. 81 (34), 5971-5979.

15. Mc DIARMID, I.B. et al. 1977, Reverse Polarity Field-Aligned Currents at High Latitudes, J. Geophys. Res. 82 (10), 1513-1518.

16. SAUNDERS, M.A. and M.J. RYCROFT 1979, Towards a more quantitative understanding of dayside magnetopause currents, Proceedings of the Sidney Chapman Conference on Magnetospheric Boundary Layers, Alpbach 11-15 June 1979, ESA Scientific and Technical Publications, SP-148, 381-384.

17. ROSENBAUER H. et al. 1975, HEOS 2 Plasma Observations in the Distant Polar Magnetosphere : The Plasma mantle, J. Geophys. Res. 80 (19), 2723-2737.

18. PASCHMANN, G. et al. 1976, Plasma and Magnetic Field Characteristics of the Distant Polar Cusp near Local Noon : The Entry Layer, J. Geophys. Res. 81 (16), 2883-2889.

19. HAERENDEL, G. et al. 1978, The Frontside Boundary Layer of the Magnetosphere and the Problem of Reconnection, J. Geophys. Res. 83 (A7), 3195-3216.

20. CROOKER, N.U. 1977, Explorer 33 Entry Layer Observations, J. Geophys. Res. 82 (4), 515-522.

21. EASTMAN, T.E. et al. 1976, The magnetospheric boundary layer : Site of plasma, momentum and energy transfer from the magnetosheath into the magnetosphere, Geophys. Res. Lett. 3 (11), 685-688.

22. Mc BRIDE, J.B. et al. 1972, Theory and Simulation of Turbulent Heating by the Modified Two-Stream Instability, Phys. Fluids 15 (12), 2367-2383.

23. FERRARO, V.C.A. 1952, On the Theory of the First Phase of a Geomagnetic Storm, J. Geophys. Res. 57 (1), 15-49.

24. WILLIS, D.M. 1971, Structure of the Magnetopause, Rev. Geophys. Sp. Phys. 9 (4), 953-985.

25. WILLIS, D.M. 1975, The Microstructure of the Magnetopause, Geophys. J.R. Astro. Soc. 41 (3), 355-389.

26. WILLIS, D.M. 1978, The magnetopause : microstructure and interaction with magnetospheric plasma, J. Atmo. Terr. Phys. 40 (3), 301-322.

27. PARKER, E.N. 1967, Confinement of a magnetic field by a beam of ions, J. Geophys. Res. 72 (9), 2315-2322.